Proc. of the 32nd International Symposium on Shock Waves (ISSW32)
doi:10.3850/978-981-11-2730-4_0502-cd

Investigations in the piston driven shock-tunnel HELM

Ch. Mundt[+], **C. Selcan**[+], **T. Sander**[+]
[+]Bundeswehr University Munich, Werner-Heisenberg-Weg, Neubiberg, 85577, Germany

Christian Mundt: christian.mundt@unibw.de

Abstract For the experimental simulation of high speed / high Mach-number flows, free piston shock-tunnels are used as a comparatively easy and cost-efficient method. At the "Universität der Bundeswehr" such a facility is operated for the investigation of aerothermodynamic characteristics of high velocity vehicles. Here, however, focus is laid on the investigation of the facility's behavior. The application of advanced measurement methods has been foreseen during the design of the tunnel. These are now used to investigate quantities during the operation in the tunnel. In the driver tube the piston dynamics is analysed by measuring the acceleration of the piston. At the end of the shock-tube, the Laser induced thermal acoustics method is used via the available optical access. Short duration, single shot measurements provide insight into the thermodynamic conditions after the shock and in front of the nozzle.

1 Introduction

The analysis of high speed / high total enthalpy flows requires a lot of research. For such conditions physicochemical effects occur, such as e.g. strong compression, chemical reactions, heating and radition. For the corresponding vehicles flying at these conditions, like scram-jets, range vehicles with continuous high flight speed and reentry bodies it is the most critical flight phase with respect to thermal and mechanical loads in most cases [**1**].

Shock-tunnels are suitable facilities to generate intermittant flows to experimentally simulate high speed / high enthalpy flows. In order to achieve the energy addition to the test gas a powerful driver is needed. It can be realised by heating the driver gas e.g. by electric discharge or deflagration/detonation. Here, however, the increase in driver gas temperature and pressure is realised by a quasi-isentropic compression using a pressurized air driven piston. This concept was introduced by [**2**] and has been further developed since. Thus, there are medium-sized facilities operated at universities like T4 at the University of Queensland in Brisbane [**3**], T5 at Caltech [**4**] and HELM at the Bundeswehr University [**5**]. More recently, T6 has commenced operation in Oxford [**6**].

The basic operational principle can be explained as follows: After installing the membranes (a thick steel one between driver and shock tube and a thin Mylar foil between shock tube and nozzle just sufficient to keep the test gas from escaping into the nozzle/test section) the main parts of the facility are closed. The desired gases are filled in the sections piston reservoir, driver and shock tube. Once the piston is released it compresses the driver gas quasi isentropically and at a predefinded pressure the steel membrane burst. A shock is released correspondingly into the test gas, and reflected at the end of the shock tube. A region of hot compressed test gas is now (almost) stagnant in front of the nozzle, destroying the tiny membrane and expanding into the test section through the nozzle, see fig. 1. The diagram displays also a position-time diagram of the basic gasdynamic processes. The numbering (e.g. region 4 in front of the piston) is used throughout the paper.

The crucial elements of the operation of the tunnel are the deceleration of the piston by the hot, compressed driver gas and the thermodynamic/chemical state of the test gas at the end of the shock tube. For the operation of the facility, its underatanding and validation of numerical

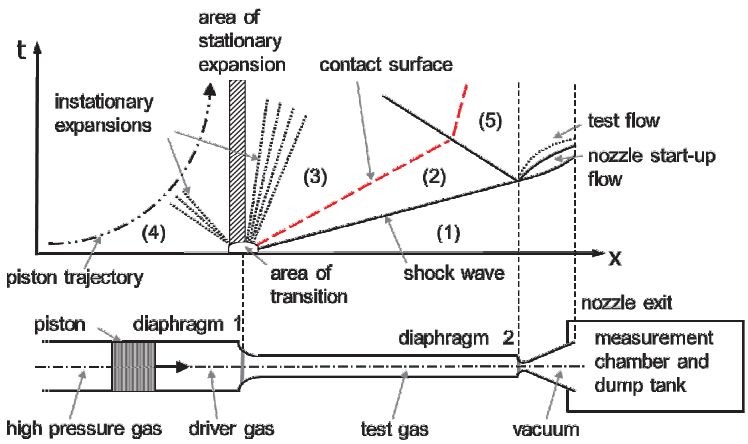

Figure 1: Schematic of the shock tunnel HELM and x,t-diagram [**7**]

methods, these conditions have to be known precisely. Thus the aim of the paper is to study the end regions of the driver and shock tubes.

The tunnel HELM has been designed to enable additional measurements of the characteristics of the tunnel itself (in addition to the usual pressure measurements). A unique feature is the optical access provided to the high pressure, high enthalpy end of the shock-tube. Additionally it is possible to fly an acclearation sensor with both of the pistons available.

In what follows some theoretical aspects needed for the paper are mentioned in chapter 2. Chapter 3 serves to detail the arrangement of the measurement configuration. The results are given and discussed in chapter 4 followed by the concluding remarks.

2 Theoretical Background

2.1 Piston dynamics

Investigations of the piston dynamics with consideration of the restrictions in the driver tube have been published [**8**, **9**, **10**].

Based on e.g. [**8**], with the definion of the compression-ratio $\lambda = \frac{L}{L_1}$ (ratio of driver tube length and the remaining length at membrane rupture) and the relation of the speed of sound a

$$\frac{a_4}{a_0} = \sqrt{\frac{T_4}{T_0}} = \lambda^{(\gamma-1)/2}, \tag{1}$$

a formula for the piston speed at the rupture of the primary membrane is obtained:

$$\frac{u_p}{a_0} = (\frac{2}{\gamma+1})^{\frac{\gamma+1}{2(\gamma-1)}} \lambda^{(\gamma-1)/2} (\frac{d}{D})^2. \tag{2}$$

u_p is the piston speed. T and γ are temperature and isentropic coefficient, while d and D are the diameters of shock and driver tubes, respectively.

Approaching the end of the driver, the piston has to be decelerated in the distance L_1. Assuming an appproximately constant pressure during this time a relation for the piston parameter P is found for tuned operation (i.e. piston comes to stand-still at the end of the driver tube):

$$P = \frac{p_4 L D^2 \pi}{4 m_p a_0^2} = \frac{1}{2}\left(\frac{2}{\gamma+1}\right)^{\frac{\gamma+1}{(\gamma-1)}} \lambda^{(\gamma-1)} \left(\frac{d}{D}\right)^4, \tag{3}$$

with p and m_p symbolizing pressure and piston mass. The equations given above are derived from gasdynamics assuming a constant isentropic coefficient. Thus they are useful for noble gases. If other gases are to be used (like e.g. air) the set of conservation equations has to be solved. Here the quasi one-dimensional method L1d is applied. It solves the 1-d Euler equations coupled to the piston motion in a Lagrangian formulation [**11**]. Empirical factors can be included for dissipative phenomena.

2.2 Laser-induced thermal accoustics

The principle of laser-induced thermal acoustics, also known as laser-induced grating spectroscopy, can be explained by opto-acoustic effects ocurring after interaction of a laser pulse with a transparent gaseous medium and is described in detail in [**12**, **13**, **14**]. Two coherent pulsed pump beams represented by the wave vectors $\overrightarrow{k_1}$ and $\overrightarrow{k_2}$ of the same magnitude and wavelength λ_{pump} cross under a certain angle Θ. Their interference generates an optical grating (grating vector $\overrightarrow{q}$), i.e. a pattern of the refraction index, in their cross-section (Fig. 2).

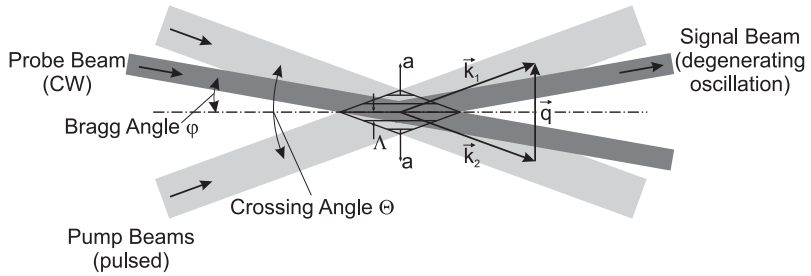

Figure 2: Schematic of the crossing laser beams.

The grating constant Λ of the induced grating can be expressed by:

$$\Lambda = \frac{\lambda_{pump}}{2\, sin\, \frac{\Theta}{2}}. \tag{4}$$

This grating can be read out by sending a third (continuous wave) laser beam (probe beam) with the wavelength λ_{probe} into the cross-section at an angle φ according to Bragg's law:

$$2\, sin\, \varphi = \frac{\lambda_{probe}}{\Lambda}. \tag{5}$$

After the interference of the two pump beams, two processes appear simultaneously and compete against each other depending on the test gas conditions and experimental settings: a non-resonant process (used for LIEGS) and a resonant process (used for LITGS).

The non-resonant process is based on the polarizability of the test gas molecules: The interference of the two crossing pump beams causes a grating of an electric field. Polarizable molecules of the test gas orient themselves toward areas of high field strength, leading to a difference in density. This density distribution causes a change of the refraction index of the test gas, resulting in an optical grating.

The resonant process implies a tunable light source to excite an electronic transition in an absorbing medium. Corresponding to the interference pattern of the beams, more gas molecules are excited in the areas of high laser intensity. A thermal grating is formed by collisional quenching of the resulting population distribution. This means that the higher energy of the excited molecules is transferred to the surrounding molecules by collision, leading to a higher temperature around formerly excited molecules. In this case, the density and thus the refraction index of the gas is changed by the influence of temperature. More details of the theory describing the governing effects for LIEGS and LITGS can be found in detail in [**13**, **14**, **15**].

Since the pump beams are pulsed, the grating only lasts for a few hundred nanoseconds. With a laser pulse length of approximately 20 ns, the lifetime of the laser-induced grating is of the order of 250 ns for temperatures in the range of 25 $^{\circ}C$ and pressures in the range of 0.1 MPa. This time scale corresponds to the theoretical temporal resolution and enables single shot measurements in shock tubes and shock tunnels. In both cases the induced acoustic waves move in opposite direction parallel to the grating vector $\overrightarrow{q}$. By alternation of constructive and destructive interference of the two waves an oscillation of the grating is formed degenerating with time. The diffraction of the probe beam occurs with the corresponding oscillation and forms the oscillating signal beam (Fig. 2). This allows the measurement of the oscillation frequency f_M, which is dependent on the speed of sound a and can be written as:

$$f_M = c\,\frac{a}{\Lambda}, \tag{6}$$

where $c = 2$ for LIEGS and $c = 1$ for LITGS, illustrating that the oscillation frequency of the electrostrictive grating is twice the frequency of the thermal grating.

For high temperatures, the isentropic coefficient γ and specific gas constant R_s become functions of temperature. Therefore equilibrium calculations have to be carried out to determine their correlation with temperature, $\gamma(T)$ and $R_s(T)$, respectively. Then temperature versus speed of sound curves have to be generated in order to determine temperatures from measured sound velocities:

$$T = \frac{a^2}{\gamma(T)\,R_s(T)}. \tag{7}$$

If chemical reactions occur, also the composition of the gas has to be taken into account.

2.3 Vibrational relaxation

It is reported [**16**], that translational and rotational degrees of freedom are excited very quickly (with in a few molecular collisions) for molecular components. The vibrational degress of freedom exhibit a relaxation time, which is several orders of magnitude higher.

Based on the work of Landau and Teller a rate equation for the population of the different energetic vibrational levels, a typical relaxation equation is obtained:

$$\frac{dE_{vib}}{dt} = \frac{E_{vibeq} - E_{vib}}{\tau}, \tag{8}$$

with E standing for energy and t for time. For "sufficiently low" temperatures [**16**] the relaxation time τ can be modelled by

$$\tau = C\frac{\exp\left(K_2/T\right)^{1/3}}{p}. \tag{9}$$

The modelling constants C and K_2 are available for oxygen, nitrogen and nitric oxide. Data for NO_2 could not be found in the literature. Thus it is assumed that the lower molecular weight nitric oxydes have a comparable relaxation time as N_2, for the time being, based on the fact that N_2 is the main constitutent of the heat-bath. The constants $C = 7.12\ 10^{-3} \mu s\, atm$ and $K_2 = 1.9\ 10^6 K$ have been used in this paper.

3 Measurement technique description

3.1 Measurement of piston acceleration

A acceleration sensor was integrated with the data recording unit is screwed to the back end of the piston (i.e. on the piston reservoir side). It begins recording after a threshold acceleration in the forward direction is reached in the experiment, and then records the acceleration and deceleration for a finite time length. After the experiment, the piston is taken out at the end of the driver tube and the data immediately retrieved for further processing.

The data recording unit was designed and made by the German-French Research Institut ISL and used on loan, which is acknowledged here.

3.2 Set-up of LITA measurements

In Fig. 3 the test setup for both the electrostrictive (LIEGS) and the thermal (LITGS) technique is shown using a frequency doubled Nd:YAG laser and a dye laser as source for the pump beams.

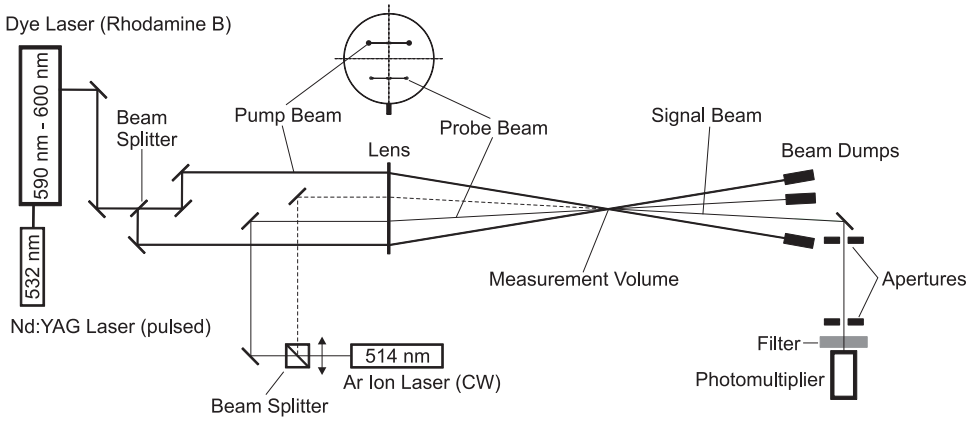

Figure 3: Schematic of the optical setup for LIEGS and LITGS.

The output beam is split by a 50:50 beam splitter. The two resulting pump beams are adjusted to equal pathlength and then pass a collecting lens. The measurement volume in the pressure cell lies in the focus of the lens and extends over several hundreds of microns. The output of a continuous wave Argon-Ion laser tuned to 514.5 nm is used as probe beam. This wavelength was chosen, because the spectral distance from the signal beam to the high-energy pump beams at 590 nm - 600 nm is big enough for their clean separation. Furthermore this line is the strongest one of the applied laser.

Additionally, a second beam splitter can be moved into the path of the probe beam to obtain a simulation of the diffracted signal beam (dashed line), which enables the alignment of the detector. The signal detection is done by a 500 MHz photomultiplier, while the data is acquired and visualized by an oscilloscope with a bandwidth of 1 GHz at 10 GS/s. To separate the signal from the reflections of the laser light, beam dumps for the two pump beams and the probe beam are used in combination with several apertures and a bandpass filter (500 nm - 550 nm) in front of the detector.

As an absorption line of a molecule in the test gas has to be excited to generate a thermal grating, a tunable narrowband dye laser pumped by a frequency doubled Nd:YAG laser is integrated into the setup to provide the pump beams. As absorbing species in the test case nitrogen dioxide NO_2 was chosen, as it is formed during experiments at HELM with concentrations up to a few percent. The excitation of NO_2 is realized in the spectral range between 590 nm and 600 nm. The mentioned wavelength range can be easily reached by using the existing frequency doubled Nd:YAG laser pumping Rhodamine B, which exhibits a high efficiency of about $\frac{1}{3}$ at 593 nm, resulting in a maximum pulse energy of about 150 mJ.

While the overall setup employed is similar to the optical setup utilized in prior small-scale shock tube studies, significantly more effort had to be invested in the laser light guiding and optical pathway, as optical access to the HELM shock tunnel is merely provided via small diameter radial bores, rather than large surface-area windows. Nozzle reservoir conditions are acquired within the orthogonal measurement plane, situated 40 mm upstream of the end wall (secondary diaphragm). LIGS measurements are carried out using both opposing, horizontal bores (180 $^\circ$ from one another) to guide pump-, probe- and signal beams into the measurement volume and again out of the shock tube section to the detector unit. Both pump beams interfere at the intersection angle Θ, giving rise to an acoustic grating located at the shock tube centreline.

Here, in addition to a geometrically closely confined laser beam pathway into and out of the measurement volume at the shock tube centerline, problems arise due to the inevitable recoil of high-enthalpy impulse facilities. Upon transient operation, compression piston acceleration and deceleration cause an axial displacement of about 30 mm of the entire shock tunnel which necessitates to guide pump, interrogation and signal laser beams in parallel to the shock tube as far as possible.

The success rate of optical measurements in earlier arrangements was strongly compromised by recessed-mounting of optical sapphire windows to the shock tube (ST) outer diameter, rather than the inner diameter [**17**, **18**], see fig. 4a. Accordingly, the high-aspect ratio (L/d 10) geometric cavities resulting from radial access bores within the nozzle reservoir section demanded laser beams to travel over large radial distance of $\approx$ 0.6 m through the stagnating test gas close to the endwall. Alignment of pump-/probe and coherent signal beam is evident to be significantly disturbed by strong secondary flow and gradual deflection, as entailed by transient compression and expansion waves, high density gradients and vortical motion. This resulted in a limited success rate of LITA single-shot measurements which ensued from strong beam steering and displacement of the coherent signal beam off the detecting photo multiplier aperture [**18**]. Recently, the employed opto-mechanical setup (i.e. coupling between optical laser components and HELM facility) has been revised such that optical sapphire windows are now flush-mounted with respect to the inner ST diameter - effectively avoiding any radial cavity. The mechanical design of both, external [**18**] and internal [**17**] shock tube windows for the highly-loaded reservoir region is illustrated in fig. 4. Both designs feature optical lenses with 500 mm focal lengths (Thorlabs) and utilize 90° turning mirrors, mounted via an external flange assembly to the shock tube outer diameter. The identical opto-mechanical assembly is used for both opposing optical access bores in order to guide laser beams into as well as out of the measurement volume at

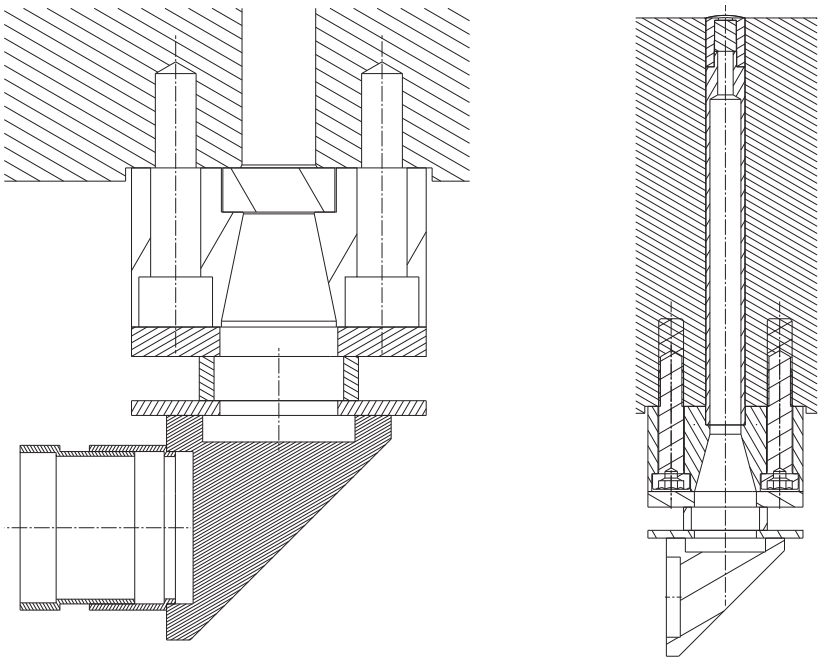

(a) External window (b) Internal window

Figure 4: Scheme of the installation of the shock-tube access windows

the shock tube centreline. In order to withstand very high reservoir pressures, most components are manufactured from steel with high tensile strength. This applies particularly to the internal window design, where high compression stress due to shock wave arrival and instantaneous pressure rise acts on the sleeve which enables wall-flush mounting of the optical window. Both external 4a and internal 4b designs utilize sapphire as window material which is favourable due to superior fracture strength and minimum absorption for relevant laser light wavelengths.

A direct improvement is a significantly enhanced geometrical beam stability which now allows better rejection of spurious reflections and stray light by smaller geometrical pinhole apertures. Accordingly, the ensuing success rate of single-shot LIGS measurements presented herein is effectively increased up to 80 %. As a side effect, inserting flush-mounted windows results in increased geometrical constriction and thus a smaller pump beam intersection half-angle $\theta/2 \approx 1.17°$ which entails an increased fringe spacing constant Λ - in contrast to a former beam crossing half-angle of $\theta/2 \approx 1.97°$ [**18**]. However, this prooves to be advantageous due to longer signal lifetimes and a longer measurement volume thus increasing measurement accuracy [**19**].

4 Discussion of results

4.1 Piston dynamics

The light-weight piston (54 kg) equipped with the measurement unit was placed into the tunnel. Its operational conditions are depicted in table 1.

Table 1: Driver conditions

Piston reservoir $[MPa]$	Driver $[MPa]$	Membrane burst pressure $[MPa]$
4	0.1	30

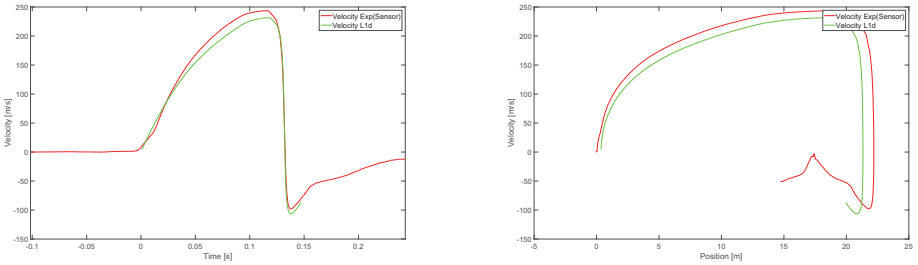

(a) Piston velocity $u_p(t)$ (b) Piston velocity $u_p(x)$

Figure 5: Piston velocity

After the experiment, the data was retrieved and the acceleration rates were integrated twice using filtering. It has to be mentioned, that at some peak deceleration spikes close to the membrane location the sensor went into saturation. Thus the integrated velocity (and length) are determined slightly on the low side.

In fig. 5a the velocity is plotted over time. Since air is used as driver gas the data has to be compared to results from L1d. Experiments with Helium as driver gas are planned for the future to enable a comparison against the parameters described in section 2.1. The maximum experimental value of the piston's speed is some 245 m/s and compares reasonably well to the computation. Especially from fig. 5b it is visible that the piston was operated untuned in this condition.

4.2 Determination of the thermodynamic conditions at the end of the shock-tube

In order to demonstrate the applicability of LIGS in the real test environment of a reflected shock tunnel facility, measurements at an enthalpy of 2.1 MJ/k) at stagnation pressures and temperatures up to some 13 MPa and 1800 K, respectively, are presented in table 2. Reference stagnation quantities in the nozzle reservoir (state 5) are predicted by CEA [**20**], using the experimentally acquired incident shock wave Mach number and assuming thermo-chemical equilibrium.

Due to minor variations of buffer pressure and main diaphragm rupture pressure ($\approx$ 22 MPa), the incident shock wave Mach number is seen to vary between 3.19 and 3.27 for the lower temperature condition. Accordingly, the post-reflected shock temperature predicted by CEA varies between 1412 and 1470 K and compare well with the measured values with a few per cent on the low side. For all cases the initial ST pressure p_1 has been maintained constant at 0.15 MPa. The inherent time delay between endwall-reflected shock wave passage and Q-switch gating was within 0.157 ms (1) and 0.148 ms (3). For the higher temperature case 3 the LITA-value is a few per cent on the high side. A sample signal is displayed in fig. 6a together with the fitted theoretical function used for temperature determination.

A further experiment was run with a time delay reduced by 20 μs for a very similar con-

Table 2: Comparison of stagnation pressure and LIGS single-shot temperature behind the reflected shock (state 5)

No.	Ma	$p_5[MPa]$		$T_5[K]$		ΔT_5	
		Th	Exp	Th	Exp	Th-Exp$[K]$	Th-Exp %
1	3.27	10.0	11.18	1470	1360.7	109.4	7.44
2	3.19	9.28	9.05	1411.5	1350.0	61.5	4.36
3	3.57	12.7	13.26	1674.7	1774.9	-98.58	-5.98

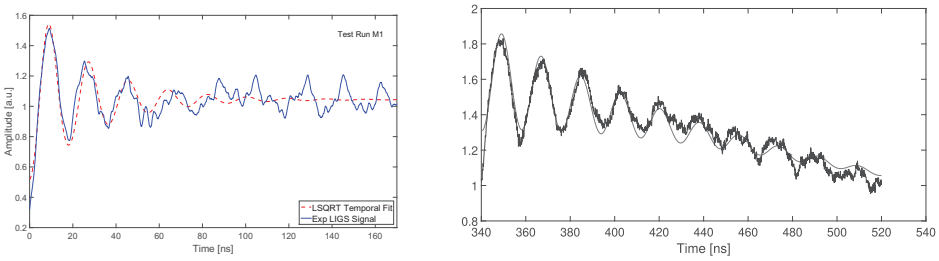

(a) Measured and fitted signals for cond.1

(b) Signals for reduced time delay

Figure 6: Sample signals from LIGS measurements

dition to 3. The unfiltered signal can be seen in fig. 6b together with the theoretical fit. The difference between theoretical value and experiment increases further with (-)188 K (equilibrium calculation 1623 K, experiment 1811 K).

5 Conclusion

In this investigation the gasdynamic conditions at the end of the driver and shock tubes of a piston driven shock tunnel are investigated. For the driver where a quasi isentropic compression is realized, the accleration of the piston was measured and analysed. In this condtion air was used as driver gas. The trajectories integrated from the acceleration values show good agreement with theoretical results. Further measurements especially with noble gases are planned for the future.

In the shock tube, the test gas air is compressed and heated by the incoming and reflected shock. After these, the temperature is predicted by postprocessing of the speed of sound, which is measured by laser induced thermal acoustics. NO_2 was used as optically active component at very small concentrations. The set-up of the measurement system had to be adapted to the specifics of a shock tunnel. During the experiments temperatures of up to some 1800K have been obtained, with good agreement to equilibrium computations. This shows, that the approach is well suited to determine the thermodynamic conditions and to explore possible conditions of thermodynamic and / or chemical non-equilibrium. The latter is focus of further research.

6 References

[1] E. H. Hirschel: Basics of Aerothermodynamics; Springer-Verlag and AIAA, Vol. 204 of Progress in Astronautics and Aeronautics, 2005.

[2] R.J. Stalker: Development of a hypervelocity wind tunnel, Aeronaut. Journ. 76, pp. 374-384, 1972.

[3] R.J. Stalker, R.G. Morgan: The University of Queensland free piston shock tunnel T4 - initial operation and preliminary calibration, Proc. 4th Nat. Aerospace Eng. Symp., Inst. Eng. Australia, 1988.

[4] H. Hornung, B. Sturtevant, J. Bélanger, S. Sanderson, M. Brouilette, M. Jenkins: Performance data of the new free-piston shock tunnel at GALCIT, Proc. 18. Int. Symp. Shock Waves, Sendai, 1991.

[5] Ch. Mundt, P. Altenhöfer: Results of HELM in initial operation as a shock tube, 10th Int. workshop on shock tube technology, Brisbane, 2011.

[6] P.L. Collen, L.J. Doherty, M. McGilvray, I. Naved, R.P.Geraets, T. Hermann, R.G. Morgan, D.E. Gildfind: Commissioning of the T6 Stalker Tunnel, AIAA 2019-1941, 2019.

[7] P. Altenhöfer: Aufbau und Anwendung eines LIGS-Meßsystems am Stoßwellenkanal HELM, PhD-thesis, Universität der Bundeswehr München, 2017.

[8] H. Hornung: The piston motion in a free-piston driver for shock tubes and tunnels, GALCIT report FM 88-1, 1988.

[9] K. Itoh: Tuned operation of a free piston shock tunnel, Proc. 20. Int. Symp. Shock Waves, Pasadena, 1995.

[10] H.Tanno, K. Itoh, T. Komuro, K. Sato: Experimental study on the tuned operation for a free piston driver, Shock Wave Journ., vol 8, pp. 1-7, 2000.

[11] P. Jacobs: Quasi-one-dimensional modelling of a free-piston shock tunnel, AIAA Journ., Vol. 32 No. 1, pp.137-145, 1994.

[12] E. B. Cummings: Laser-induced thermal acoustics: simple accurate gas measurements, Optics Letters, Vol. 19, No. 17, 1 Sep. 1994, pp. 1361-1363.

[13] E. B. Cummings, I. A. Leyva, H. G. Hornung: Laser-induced thermal acoustics (LITA) signals from finite beams, Applied Optics, Vol. 34, No. 18, 20 Jun. 1995, pp. 3290-3302.

[14] A. Stampanoni-Panariello: Laser-Induced Gratings in the Gas Phase: Formation Mechanisms and Applications for Diagnostics, Ph.D. Dissertation, Swiss Federal Institute of Technology Zurich (ETH Zurich), Switzerland, 2003.

[15] R. W. B. Pearse, A. G. Gaydon: The Identification of Molecular Spectra, 4^{th} ed., Chapman

and Hall, London, 1976.

[16] W.G. Vincenti, C.H. Kruger: Physical gas dynamics, J. Wiley, New York, 1967.

[17] C. Selcan, T. Sander, P. Altenhöfer, F. Koroll, Ch. Mundt: Stagnation Temperature Measurements in a Shock-Tunnel Facility using Laser-Induced Grating Spectroscopy, AIAA Journal of Thermophysics and Heat Transfer Vol. 32, No. 1, pp. 1-11, 2017.

[18] P. Altenhöfer, T. Sander, F. Koroll, Ch. Mundt: LIGS Measurements in the Nozzle Reservoir of a Free Piston Shock Tunnel, Shock Waves Vol. 29, No. 2, pp. 307-320, 2017.

[19] S. Schlamp, T. Rösgen, D.N. Kozlov, C. Rakut, P. Kasal, J. von Wolfersdorf: Transient Grating Spectroscopy in a Hot Turbulent Compressible Free Jet, Journal of Propulsion and Power Vol. 21, No. 6, pp. 1008-1018, 2005.

[20] B. J. McBride, S. Gordon: Computer Program for Calculation of Complex Chemical Equilibrium Compositions and Applications: Part II: User's Manual and Program Description, Report Number NASA RP-1311-P2, 1996.